Arecibo Technical & Operations Memo ATOMS 2000-03

MAIN BEAM AND FIRST SIDELOBE PARAMETERS FOR ARECIBO'S RECEIVER SYSTEMS

Carl Heiles, Phil Perillat, Michael Nolan, Duncan Lorimer, Ramesh Bhat, Tapasi Ghosh, Ellen Howell, Murray Lewis, Karen O'Neil, Chris Salter, Snezana Stanimirovic

ABSTRACT

During September 2000 we made extensive observations of the main beam and first sidelobes for all of Arecibo's receiver systems. For each system, we characterize the main beam and sidelobe in all Stokes parameters employing parameters that allow reconstruction of the complete beam patterns and, also, afford an easy way to see how the beam changes with azimuth, zenith angle, and time. For the main beam in Stokes I the parameters include the beam width, ellipticity and its orientation, coma and its orientation, the point-source gain, the integrated gain (or, equivalently, the main beam efficiency); for the other Stokes parameters the beam parameters include beam squint, and beam squash. For the first sidelobe ring in Stokes I the parameters include an 8-term Fourier series describing the height, radius, and radial width; for the other Stokes parameters they include only the sidelobe's fractional polarization.

The main beam width is smaller and the sidelobe levels higher than for a uniformly-illuminated aperture of the same effective area. These effects are modeled modestly well by a blocked aperture, with the blocked area equal to about 10% of the effective area. The gain and main beam efficiency are affected by telescope imperfections even near 1 GHz. At 1175 MHz, the beam efficiency ≈ 0.56 and the first sidelobe efficiency ~ 0.20; the total ~ 0.75, which is equal to the ratio of antenna temperature to brightness temperature for a uniformly bright source whose size extends to the edge of the first sidelobe. These quantities and the on-axis gain depend on azimuth as well as zenith angle. Things get worse at higher frequencies, as illustrated by Figure 2 and Table 2.

1. INTRODUCTION

In ATOMS 99-02 and 2000-02 we measured the properties of the Arecibo Observatory 1.15-1.73 GHz (L-Band Wide or LBW) feed at 1420 MHz, where the observation pattern included two 13-point crosses, one aligned with the azimuth and zenith angle directions $(\hat{az}, \hat{za})$ and one at 45° to $(\hat{az}, \hat{za})$. That observing pattern is inefficient in observing time and, moreover, restrictive because it doesn't continuously sample along a radial cut through the beam.

The current effort was directed towards characterizing all receivers and establishing a historical record so that the beam patterns can be monitored as future improvements in the telescope structure occur. We devised a new observing pattern that greatly improves both the observing efficiency and the sampling completeness. It consists of four continuously sampled scans oriented every 45° with respect to $(\hat{az}, \hat{za})$ yielding an 8-pointed star-shaped pattern that extends out to three nominal HPBW (Half Power Beamwidths) on each side of the nominal pointing position. These data allow parameterization of the main beam and first sidelobe as described in the following sections. We begin in §2 by describing the parameterization scheme for Stokes I. §3 presents samples of observational results for the most important parameters involving Stokes I and compares them with a theoretical model of a uniformly-illuminated blocked circular aperture. §4 describes observational results for the more esoteric main beam parameters ellipticity and coma. §5 presents results on the first sidelobe. §6 describes the parameters beam squint and squash for the other Stokes parameters, and also presents results; §7 provides grey-scale images of the beam in the four Stokes parameters for a particular (az, za).

We compute results for the following feeds: 430 MHz Line Feed (430CH), 430 MHz Gregorian (430G), 1.15-1.71GHz (L-Band Wide, or LBW), 1.27-1.53 GHz (L-Band Narrow, or LBN), 2.33-2.43 GHz (S-Band Narrow or SBN), and 4-6 GHz (C-Band, or CB).

2. PARAMETERIZATION OF THE STOKES I BEAM

2.1. Five Parameters that Describe the Main Beam Shape

We follow Rohlfs and Wilson's (2000) definition of the normalized main-beam power pattern, $P(\theta,\phi)_n = \frac{P(\theta,\phi)}{P_{max}}$. We represent it with five parameters of a two-dimensional Gaussian defining a power pattern with ellipticity and coma. The parameters are the average beamwidth Θ_0, beam ellipticity Θ_1 with an orientation $\phi_{\rm beam}$, and coma $\alpha_{\rm coma}$ with orientation $\phi_{\rm coma}$.

To parameterize the elliptical beam, we take the ratio of major to minor axes to be $\frac{\Theta_0+\Theta_1}{\Theta_0-\Theta_1}$ with the major axis oriented at position angle $\phi_{\rm beam}$, and the beamwidth Θ to vary as

$$\Theta = \Theta_0 + \Theta_1 \cos 2(\phi - \phi_{\rm beam}) \ . \tag{1}$$

where ϕ is the position angle in the (az, za) coordinate system, defined to be zero along the positive azimuth axis and increase towards positive zenith angle (see Figure 1).

We parameterize the coma lobe with a function chosen for analytical convenience; it is not based on a proper derivation. The parameters are the coma strength $\alpha_{\rm coma}$ and its position angle $\phi_{\rm coma}$. We assume that the effect of coma depends only on the projection of θ along the coma direction; this distance is

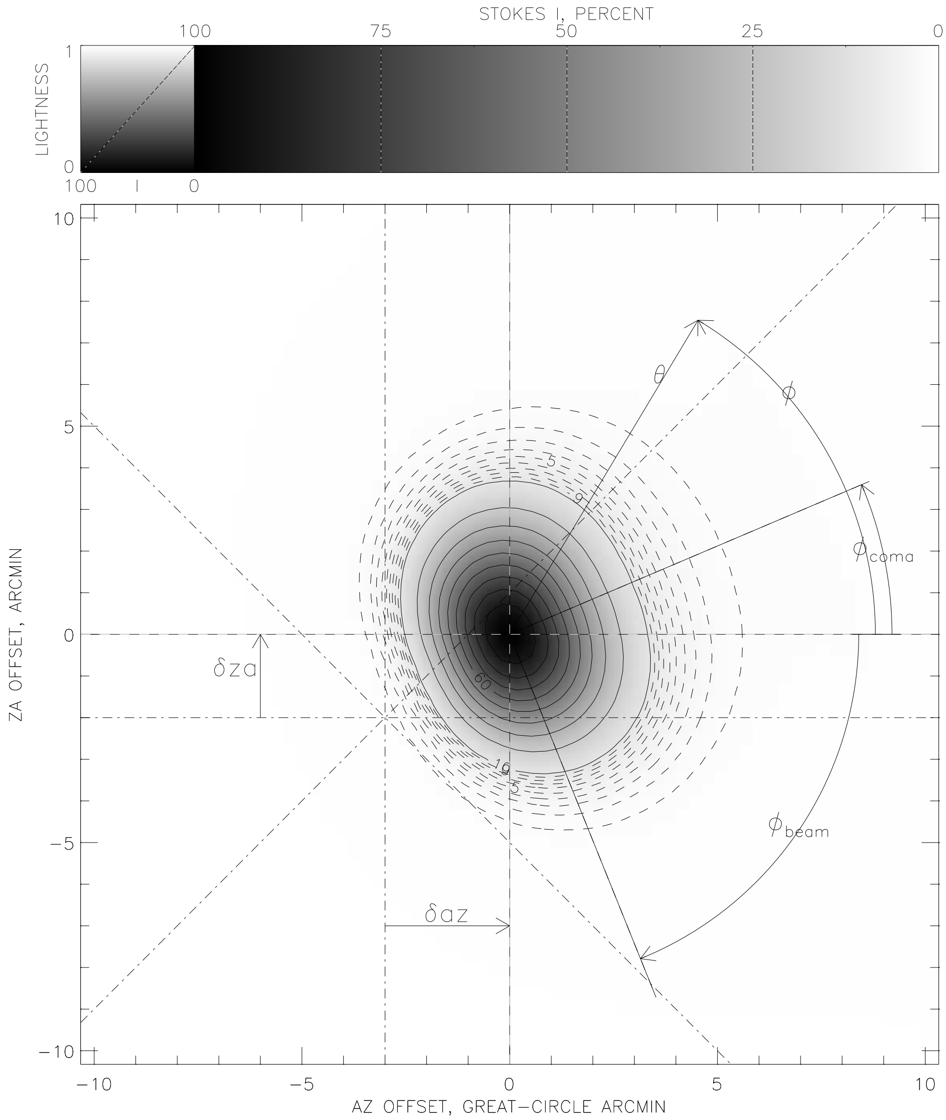

Fig. 1.— Grey-scale/contour image of a main beam having $\alpha_{\rm coma} = 0.2$, $\phi_{\rm coma} = 22.5°$, $\Theta_0 = 3.4$ arcmin, $\Theta_1 = 1$ arcmin (both Θ's are *HPBW* in this figure), and $\phi_{\rm beam} = -67.5°$. The dashed lines intersect the true beam center; the dashed-dot lines intersect the assumed (from the telescope pointing) beam center, and are the paths of the telescope in the observing pattern. Solid contours are $(0.1, 0.2, \ldots)$ of the peak; dashed contours are $(0.01, 0.02, \ldots)$.

$$\theta_{\rm coma} = \theta \cos(\phi - \phi_{\rm coma}) \ . \tag{2}$$

The normalized power distribution including parameterized ellipticity and coma is then:

$$P_n = \exp\left(- \frac{\theta^2 \left(1 - \min\{\alpha_{\rm coma} \frac{\theta_{\rm coma}}{\Theta_0}, 0.75\}\right)}{\Theta^2} \right) \tag{3}$$

where θ is the great-circle angular distance of the position from the *true* beam center, equal to $\sqrt{az^2_{\rm offset} + za^2_{\rm offset}}$. The term $\min\{\alpha_{\rm coma} \frac{\theta_{\rm coma}}{\Theta_0}, 0.75\}$ is included to prevent the coma term from unduly distorting the beam far from the center. Note that the beamwidth Θ related to the usual half-power beamwidth by $HPBW = 2(\ln 2)^{1/2}\Theta \approx 1.665\Theta$.

Figure 1 illustrates these quantities with a main beam having severe coma and exaggerated ellipticity. In this example, $\alpha_{\rm coma} = 0.2$, $\phi_{\rm coma} = 22.5°$, $\Theta_0 = 3.4$ arcmin, $\Theta_1 = 1$ arcmin, and $\phi_{\rm beam} = -67.5°$.

2.2. Relating the Beam to the Observation Pattern

When observing the beam shape we must point the telescope to an assumed beam center. The four scans of the observing pattern intersect this assumed beam center, as shown by the dash-dot lines on Figure 1. The difference between the assumed and actual centers is the pointing offset. Thus, in equation 3,

$$az_{\rm offset} = az_{\rm obs} + \delta az \tag{4a}$$

$$za_{\rm offset} = za_{\rm obs} + \delta za \tag{4b}$$

where $(az_{\rm obs}, za_{\rm obs})$ are the "observed" offsets, that is the ones measured with respect to the assumed center.

2.3. The First Sidelobe in Stokes I

Detailed maps of the first sidelobe show some azimuthal structure (i.e., with ϕ on Figure 1). Our observing pattern provides four radial cuts through the beam. We least-squares fit each radial cut with three Gaussians, two weak ones at the beginning and end for the sidelobes and a strong one for the main beam. This yields values of the sidelobe height, center, and width at 8 ϕ's. We Fourier transform each of these three parameters and reconstruct the sidelobe using N Fourier coefficients, with $N \leq 8$. Using $N < 8$ is equivalent to performing a least-squares fit on the 8 ϕ's and deriving N coefficients, which is not unreasonable because the fitting process is hardly perfect. In practice, on the basis of the maps shown in ATOMS 2000-02 we adopt $N = 6$, which is just sufficient to reveal the blockage of the triangle structure.

This procedure is complicated in practice. In some cuts the sidelobe is absent or is not well-fit. We test each derived sidelobe Gaussian fit and accept it only if its width is smaller than the nominal $HPBW$and greater than 0.3 times the nominal $HPBW$. We also require the fractional uncertainty in the derived intensity to be less than 0.45. In cases having no acceptable fit, we take the height equal to zero, and take the center and width equal to the average of all the other acceptable centers and widths for that particular group of cuts.

With this fitting procedure, the main beam and first sidelobe are unambiguously defined and we can compute the beam efficiency for each.

2.4. Effective Area, On-Axis Gain, and Beam Efficiencies

Again we follow Rohlfs and Wilson (2000) and define the directive gain G as the gain relative to an isotropic radiator for a single polarization. Here we are concerned with treating polarization, for which purpose we must explicitly define the *unsubscripted* directive gain to apply to $\frac{\text{Stokes I}}{2}$; below we will subscript it with a polarization label. Conservation of energy requires that G satisfy the relationship

$$\int\int_{\text{whole sky}} G d\Omega = 4\pi \ . \tag{5}$$

The on-axis point-source directive gain is directly related to the effective area A_{eff} by

$$G_{\text{max}} = \frac{4\pi A_{\text{eff}}}{\lambda^2} \ , \tag{6}$$

and in practical units of source flux in Jy, area in m^2 we have

$$KperJy = 10^{-26} \frac{A_{\text{eff}}}{2k_B} \tag{7}$$

or

$$A_{\text{eff}} = 2 \times 10^{26} k_B KperJy \tag{8}$$

so, eliminating A_{eff}

$$\begin{aligned} G_{\text{max}} &= \frac{4\pi(2 \times 10^{26} k_B KperJy)}{\lambda^2} && (9) \\ &= \frac{3.47 \times 10^8 KperJy}{\lambda_{\text{cm}}^2} && (10) \end{aligned}$$

where λ_{cm} is the wavelength in cm. Arecibo's theoretical gain, without blockage, is $KperJy \approx 11$, which is equivalent to a uniformly illuminated circular aperture with radius 94 m. The normalized power pattern P_n, which we used above in equation 3, is just

$$P_n = \frac{G}{G_{\rm max}} = 2.89 \times 10^{-9} \frac{G \lambda_{\rm cm}^2}{K per\, Jy} \ , \tag{11}$$

so

$$\int\int_{\rm whole\ sky} P_n d\Omega = 3.62 \times 10^{-8} \frac{\lambda_{\rm cm}^2}{K per\, Jy} \ . \tag{12}$$

The "efficiency" of a portion of the telescope's beam is defined as the integral of its directive gain divided its integral over the whole sky. Thus, using units of arcmin^2 for Ω and cm for λ,

$$\eta_{\rm beam} = 2.34 \frac{K per\, Jy}{\lambda_{\rm cm}^2} \int\int_{\rm beam} P_n d\Omega_{\rm arcmin^2} \ . \tag{13}$$

Normally we consider the main beam efficiency, but we can also use the same terminology for the sidelobes. The main beam and first sidelobe integrals are, in principle, expressible analytically by our parameterization scheme; in practice, however, we compute them numerically.

3. COMPARISON WITH A THEORETICAL MODEL: A UNIFORMLY-ILLUMINATED CIRCULAR APERTURE HAVING BLOCKAGE

It is instructive to compare Arecibo's beam pattern with a theoretical model. The most convenient is a uniformly-illuminated circular aperture, whose parameters we denote by the subscript U. We will then consider a circular aperture with a central circular blockage. Even though Arecibo's beam is elliptical, it's close enough to circular that the model makes physical sense and the deviations from circular are modest.

3.1. A Uniformly-Illuminated Unblocked Circular Aperture

The electric field pattern of an unblocked aperture is

$$F(\sin\theta) = 2\frac{J_1(u)}{u}, \tag{14}$$

where

$$u = \frac{\sin\theta}{(\theta_d/\pi)} \quad \text{and} \quad \theta_d = \lambda/D$$

(Rohlfs and Wilson 2000). The field for a blocked aperture is a suitably-weighted arithmetic combination of different diameters. In principle, the best way to fit this model to the data is to compare the observed and theoretical beam shapes. However, this is not so easy because of Arecibo's elliptical beam. Rather, we examine five parameters. Of these, two are *robust* in the sense that they don't depend on assuming a perfectly smooth reflecting surface for the bowl and, in addition, don't depend on knowing an accurate source flux or a noise diode calibration standard (cal) temperature. The robust parameters specify only the beam shape using ratios of the first sidelobe and main beam.

We first consider an "ideal" uniform illumination pattern by numerically integrating Equation 14. These "ideal" values are additionally subscripted I. The peak power in the first sidelobe (FS), as a fraction of the peak of the main beam (MB) (which is unity by definition) is

$$P_{n,FS,U,I} = 0.0175 \tag{15a}$$

and the ratio of beam efficiencies as defined by equation 13 is

$$\left(\frac{\eta_{FS}}{\eta_{MB}}\right)_{U,I} = 0.0861 \ , \tag{15b}$$

Obviously, these two parameters are not independent because, to some extent, they measure the same thing.

In the same way we can compute three *non-robust* parameters,

Half-power beam width:

$$(HPBW)_{U,I} = \ 0.597 \frac{\lambda_{cm}}{KperJy^{1/2}} \text{ arcmin.} \tag{16a}$$

Main beam efficiency:

$$(\eta_{MB})_{U,I} = 0.840 \ , \tag{16b}$$

And, combining equations 16b and 15b to get the total efficiency in the main beam and first sidelobe:

$$(\eta_{MB} + \eta_{FS})_{U,I} = 0.840(1 + 0.0861) = 0.912 \ . \tag{16c}$$

To calculate $HPBW$ in equation 16a we use diameter $d_{\rm eff} = \sqrt{\frac{4A_{\rm eff}}{\pi}}$ and the $HPBW$ for a uniformly-illuminated aperture, $HPBW = 1.03\frac{\lambda}{d_{\rm eff}}$. For the data, the observed $HPBW$ is derived from the Gaussian fit, and the value expected from the model is derived from the effective area $A_{\rm eff}$, which is in turn derived directly from $KperJy$, namely from observations of calibration sources with known flux using a standard noise diode. This dependence on $KperJy$ is what makes these parameters non-robust, because $KperJy$ is affected by telescope imperfections (surface roughness and subreflector misalignment), loss in waveguide feeds, errors in source calibrator flux, and errors in noise diode calibration temperature.

Our beam parameterization is done through Gaussian fits to the data, and thus we should compare those fits with Gaussian fits to the ideal uniform illumination pattern. Gaussian fits don't represent the theoretical model perfectly, but we can compute correction factors P_{FS}, E_{FS}, and E_{MB}, and H for the Gaussian fits to the ideal uniform circular aperture. The Gaussian fit-derived parameters are unsubscripted, as they are used in all further analysis.

These correction factors are the ratio of the (unsubscripted) fit parameters to the ideal parameters, (subscripted I):

$$H = \frac{HPBW_U}{HPBW_{U,I}} \tag{17a}$$

$$E_{MB} = \frac{\eta_{MB,U}}{\eta_{MB,U,I}} \tag{17b}$$

$$E_{FS} = \frac{\eta_{FS,U}}{\eta_{FS,U,I}} \tag{17c}$$

$$P_{FS} = \left(\frac{P_{n,FS,U}}{P_{n,FS,U,I}}\right) . \tag{17d}$$

Note that these coefficients only scale the Gaussian fit to the integration; the results of the integration itself with blockage can be quite different than the unblocked case, and will be discussed in § 3.4.

Table 1: FACTORS IN EQUATIONS 17 VERSUS BLOCKAGE

FACTOR//BLOCKAGE	0	10%	20%
H	0.961	0.955	0.952
P_{FS}	1.038	1.038	1.033
E_{MB}	1.060	1.067	1.070
E_{FS}	0.865	0.925	0.947

Table 1 gives values of the (H, P, E) parameters in equation 17 for the unblocked case (0%) and for two different blocked cases with 10% and 20% blockage. For example, multiplication of the ideal $HPBW_{U,I}$ by H gives $HPBW_U$, the value that is derived from a Gaussian fit to the ideal beam shape, and thus can be compared directly to a Gaussian fit to telescope data. The ideal beam is wider at the top and falls more rapidly than the Gaussian; this makes $H < 1$ for a uniformly-illuminated aperture with no blocking. Empirically, the values change slowly with blockage, so that these few choices describe most reasonable situations.

3.2. Representative Observed Parameter Values

Table 2 provides representative observed values for the above-defined parameters. Some commentary:

(1) az dependence: While Arecibo's design is such that the telescope performance depends on za, it is also found to depend on az—as do our parameters. The az dependence becomes stronger with increasing frequency, but is even noticeable for LBW. Figure 2 shows representative behavior.

(2) frequency dependence of $HPBW$: If we take the $HPBW$ at 1175 MHz as a reference and calculate expected $HPBW$s by scaling with the wavelength, we find that the systems have higher $HPBW$ by the following ratios: 430CH, 0.802; 430G, 1.00; LBW (1415 MHz), 1.02; LBW (1666 MHz), 1.03; SBN, 1.07; CB, 1.20. The low value for 430CH occurs because the line feed illuminates a much larger area than does the Gregorian subreflector. The higher values for SBN and CB indicate that these systems illuminate smaller areas than the LBW system, or that large-scale surface imperfections or defocusing broadens the beam.

(3) frequency dependence of $KperJy$ and related quantities: The LBW system performance is significantly better at 1175 MHz than at 1415 MHz, as is well-documented by Phil's web page. This is not an effect of illumination or blockage, because the $HPBW$s are very close to the wavelength ratios and the $\frac{\eta_{FS}}{\eta_{MB}}$ ratios are almost identical. Beam efficiencies are closely related to $KperJy$, but change less drastically—as expected, because they integrate the beams over solid angle. While frequency dependence of the cal could be a factor, this shows that the reflector surface roughness plays a role even at these low frequencies.

(4) frequency dependence of $P_{n,FS}$: As we discuss below, this parameter depends on three quantities: illumination taper, blockage, and the combination of large-scale surface irregularities and subreflector misalignment. SBN has the smallest $P_{n,FS}$, which indicates that its illumination taper is more severe than for the other systems.

3.3. Comparison of Observations with the Unblocked Aperture

From the above, we see that surface inaccuracy affects telescope performance even for LBW. Our robust parameters don't seem to be much affected, except perhaps at CB, but we wish to look at the complete set. Therefore, we begin by restricting our attention to the two lowest frequencies, 1175 and 430 MHz.

Table 3 compares some of the observed parameters with those predicted for an unblocked aperture (equations 15 and 16). Arecibo's beam doesn't agree at all with these values. In particular, consider the two robust parameters. These describe the ratio of powers of the first sidelobe and main beam and they are higher by factors ranging from 2.2 to 4.7. Conventional feeds, such as LBW, produce a tapered illumination, which *decreases* the sidelobe level relative to the uniformly illuminated case. It is impossible to *increase* the sidelobe level without introducing a relative decrease in the center of the illumination pattern—a donut-like pattern. For the Gregorian, this occurs naturally because of blockage of the primary reflector by the central support structure. For the 430CH feed, it is a result of the line-feed illumination pattern. We can use

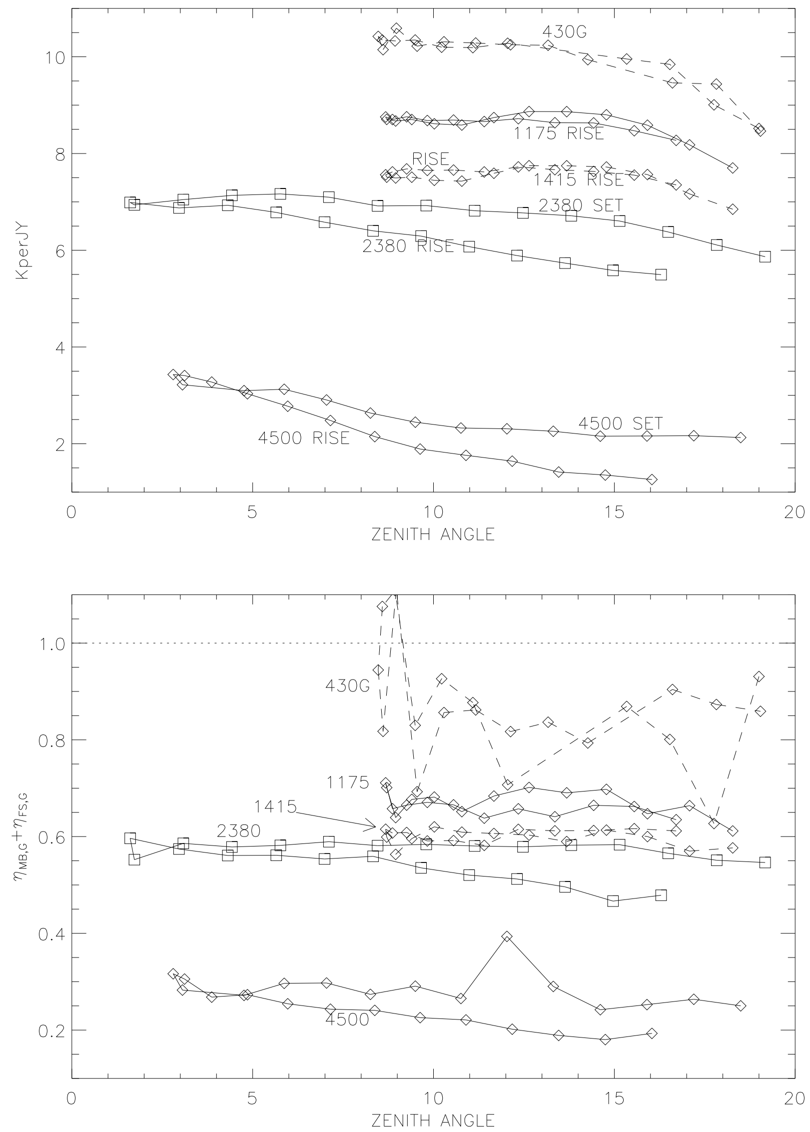

Fig. 2.— (az, za) dependence of $KperJy$ and $\eta_{MB} + \eta_{FS}$ (the sum of the main beam and first sidelobe efficiencies) for four receivers (two LBW frequencies). In order of decreasing frequency the sources are: B1634+269, B1749+096, B1749+096, B2249+185, B1615+212. The two LBW frequencies were taken simultaneously on B1749+096, which is a variable source with unknown flux; we tied its $KperJy$ to that of B1634+269 at $za = 10°$.

Table 3 to estimate the fraction of blocked area for LBW.

Table 2: REPRESENTATIVE OBSERVED PARAMETER VALUES

RCVR	FREQ	SOURCE	za	$P_{n,FS}$	$\frac{\eta_{FS}}{\eta_{MB}}$	$KperJY$	$HPBW$	η_{MB}	$\eta_{MB}+\eta_{FS}$
430CH	430	B2249+185	5	.039	0.24	16.5	8.7	0.69	0.85
430G	430	B1634+269	10	.039	0.33	10.3	10.9	0.66	0.88
LBW	1175	B1634+269	10	.043	0.32	8.7	4.0	0.56	0.75
LBW	1415	B1634+269	10	.046	0.32	7.5	3.4	0.50	0.67
LBW	1666	B1634+269	10	.042	0.31	6.9	2.9	0.48	0.62
LBN	1415	B1634+269	10	.048	0.31	7.2	3.4	0.48	0.62
SBN	2380	B2249+185	10R	.026	0.18	6.3	2.1	0.46	0.54
SBN	2380	B2249+185	10S	.026	0.18	6.9	2.1	0.50	0.58
CB	4500	B1615+212	10R	.073	0.47	1.8	1.15	0.15	0.22
CB	4500	B1615+212	10S	.037	0.21	2.4	1.18	0.22	0.28

za is in degrees and $HPBW$is in arcmin. For SBN and CB we provide values at two azimuths. The suffixes (R, S) on zamean "Rise" and "Set", respectively. *We emphasize that all values are representative*: values change both with az and za!

Table 3: COMPARISON OF OBSERVED AND UNBLOCKED MODEL PARAMETERS

RCVR	FREQ	$\frac{P_{FS}}{(P_{FS})_U}$	$\frac{\eta_{FS}}{\eta_{MB}}/(\frac{\eta_{FS}}{\eta_{MB}})_U$	$d_{\rm eff}$	$\frac{HPBW}{(HPBW)_U}$	$\frac{\eta_{MB}}{(\eta_{MB})_U}$	$\frac{\eta_{MB}+\eta_{FS}}{(\eta_{MB}+\eta_{FS})_U}$
430CH	430	2.2	3.4	241	0.88	0.78	0.89
430G	430	2.2	4.7	190	0.87	0.74	0.92
LBW	1175	2.4	4.6	175	0.80	0.63	0.79
LBW	1415	2.5	4.6	162	0.75	0.56	0.70

3.4. The Effects of Blockage

We calculate blockage by subtracting the voltage pattern of a circular blocking aperture from that of the illuminated aperture, taking care to keep the power ratio equal to the area ratio. We keep the effective area constant, because that's what our observations provide. We normalize the voltage at the center of the effective area's pattern to unity and plot the above quantities versus $\frac{\text{blocked area}}{\text{effective area}}$ in Figure 3. For comparing with observations we assume that the blocked radiation is scattered into the sky, not absorbed, so that equation 5 holds; this reduces η_{MB} by $\frac{\text{effective area}}{\text{illuminated area}}$ relative to the assumption that the blocked radiation is absorbed. Recall that, according to Babinet's principle, the effect of geometrical blockage is doubled; below we will derive blockage $\sim 10\%$, which corresponds to physical blockage $\sim 5\%$.

Figure 3 exhibits plots of the parameters versus the fractional blocked area. Xs on these

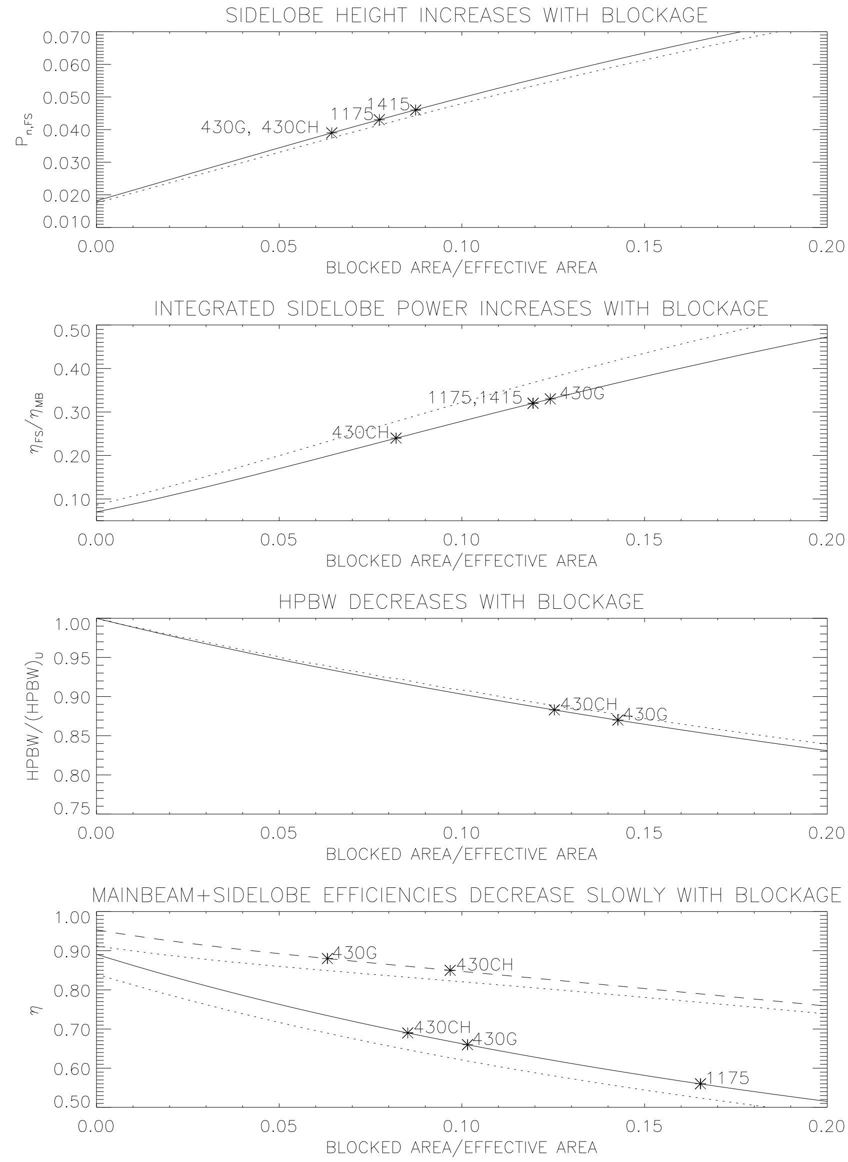

Fig. 3.— Blockage-sensitive, measurable parameters versus the ratio of blocked area to effective area. Solid lines show the Gaussian parameters as are derived by fitting the main beam and first sidelobe; dotted lines show the actual parameters for the theoretical model. The top two frames show the robust parameters: the first sidelobe peak amplitude (relative to the main beam peak) and the ratio of the integrated first sidelobe to main beam power. The third and fourth show the non-robust parameters: the *HPBW* relative to that of an unblocked aperture and the beam efficiencies of the main beam and, also, main beam plus first sidelobe.

plots show the measured quantities; the points are placed vertically using the observed value and horizontally using the curves. Thus, the "derived" blockages $\frac{\text{blocked area}}{\text{effective area}}$ that correspond to the model can be read off of the horizontal axes. The "derived" blockages have wide scatter. However, this is not unexpected.

First consider the robust parameters in the two top frames. The 430CH illuminated area is much greater than the LBW area, so if the blockage is geometrical then the blockage at 430CH should be 0.55 times that at 1175; instead, the factors are (0.86, 0.69) from the top two frames, respectively. These higher ratios mean that the sidelobe height for 430CH is higher than it would be for pure geometric blockage. The reason is probably the donut illumination pattern of the 430CH line feed. Not surprisingly, we cannot use the 430CH points to estimate geometrical blockage for the Gregorian feeds, as the illumination pattern is quite different.

For the robust parameters in LBW, the blockages lie somewhat below and above 0.10 in the top two frames, respectively. It seems reasonable to adopt a blockage of 0.10 for discussion purposes. In the following section we introduce equation 18 and Figure 4, which treat this particular blockage specifically. We assume that this is geometrical, so for 430CH, with its larger illumination pattern, the blockage should be 0.056.

3.5. Approximate Equations Describing 10% Blockage

Above, we found that a 10% blocked aperture crudely approximates Arecibo's aperture for Gregorian feeds. For this particular blockage, Figure 4 exhibits the beam shape and, also, the Gaussian fit.

The Gaussian is a reasonably accurate rendition of the theoretical model, but has its faults: it doesn't fall to zero between the main beam and the sidelobe and it doesn't reproduce the details of the shape very well. Then again, neither the Gaussian nor the model fits the data particularly well. In fact, they cannot possibly do so because the sidelobe structure changes with ϕ, while the model is circularly symmetric. An additional limitation of both our parameterization and our model is the neglect of additional sidelobes, which contribute non-trivially to the total beam efficiency.

We adopt this particular model, namely the uniformly illuminated circular aperture with 10% blockage, as a standard for comparison of telescope performance at different wavelengths.

We observationally evaluate the parameters and compare them to the following standard set of parameters, which we define to be the "standard model". We obtain the standard model by re-integrating equation 14 including 10% blockage, and, along with the Gaussian fitting correction coefficients in the "10%" column of Table 1, rewrite equations 15 and 16 as

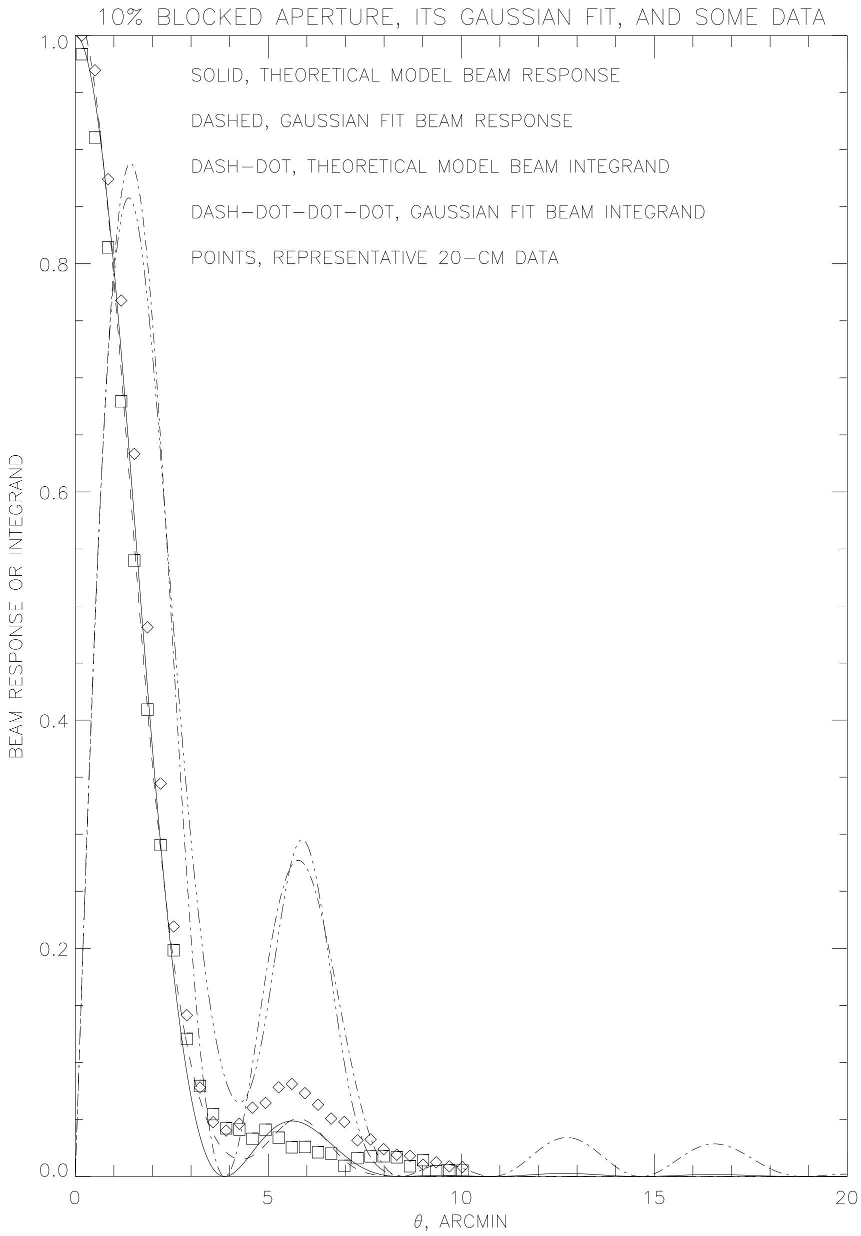

Fig. 4.— Normalized power pattern P_n, and also the integrand θP_n, for **(1)** the standard model of a uniformly illuminated 10% blocked aperture (solid, dash-dot lines), and **(2)** its Gaussian-fit counterpart (dash, dash-dot-dot-dot lines). The squares and diamonds are representative data points for P_n from the LBW feed at 1415 MHz, obtained by averaging different cuts in one single observing pattern.

$$(HBPW) = H\ 0.541 \frac{\lambda_{\rm cm}}{Kper\,Jy^{1/2}} = 0.517 \frac{\lambda_{\rm cm}}{Kper\,Jy^{1/2}}\ \text{arcmin} \tag{18a}$$

$$(P_{n,FS}) = P_{FS}\ 0.0486 = 0.0504 \tag{18b}$$

$$(\eta_{MB}) = E_{MB}\ 0.617 = 0.658 \tag{18c}$$

$$\left(\frac{\eta_{FS}}{\eta_{MB}}\right) = \left(\frac{E_{FS}}{E_{MB}}\right) 0.327 = 0.284\ , \tag{18d}$$

$$\eta_{MB} + \eta_{FS} = E_{MB}\ 0.617 + E_{FS}\ 0.202 = 0.845\ . \tag{18e}$$

The numerical values given at the extreme right in each equation are the Gaussian fit parameters, obtained by using the factors (H, P, E) from the middle column in Table 1.

We emphasize that this standard model applies only in the limit of long wavelengths, where telescope imperfections are negligible. We hope that, eventually, Arecibo's performance will improve to this standard over much of the currently used wavelength range, but at the present time the performance approaches this standard only below 1 GHz. Specifically, we expect departures from this standard model as follows:

(1) Most feed systems don't provide uniform illumination; rather, the illumination is tapered. Tapering increases $HPBW$ and η_{MB} and decreases sidelobe levels, which is opposite to blockage. Thus, the actual geometrical blockage must be somewhat larger than our adopted 10%. Because these two effects work in opposite directions, we surmise that the relationships among our derived parameters (such as $HPBW$ and η) remain approximately correct.

(2) For 430CH the line feed illuminates almost the entire aperture at zenith, reducing $\frac{\text{blocked area}}{\text{effective area}}$ to about 0.056. Because the illumination differs completely from the illumination provided by the Gregorian feeds, 430CH should not be compared with this standard model.

(3) Above 1 GHz, imperfections in the telescope surface become increasingly important. If these imperfections are random, then they scatter radiation away from the main beam according to the Ruze (1966) formulation and will decrease $Kper\,Jy$ and all beam efficiencies η. Using this reduced $Kper\,Jy$ may make equation 18 provide a $HPBW$ that is too large. The ratio of FS to MB should not be affected much unless the correlation lengths of the surface imperfections are large—but, of course, there *do* exist some large scale correlations.

(4) Above 1 GHz, large-scale imperfections in the telescope surface and, also, in the mirror alignment become important. These produce significant changes in near-in sidelobes. Two well known effects are (1) the grating-like response caused by the periodic surface irregularity of the bowl, and (2) the coma lobe. These effects decrease $Kper\,Jy$, increase $HPBW$, probably increase the first sidelobe power, and put some of the main beam power into near-in sidelobes. We expect $\eta_{MB} + \eta_{FS}$ to decrease, but their power to go primarily into near-in sidelobes so that the antenna temperature for an extended source will not decrease very much. Of course, the detailed behavior is complicated, and in addition small-scale random surface irregularities also become important.

3.6. A More Accurate Determination of Blockage

Suppose that the blockage is really 10% so that equation 18a holds. The $KperJy$ appearing there is an ideal one that obtains in the case of no surface irregularities or subreflector misalignments; we denote this idealized value by $KperJy_{ideal}$. The *actual* $KperJy$ approaches (and, hopefully, will someday equal) $KperJy_{ideal}$ at low frequencies, where telescope imperfections become unimportant.

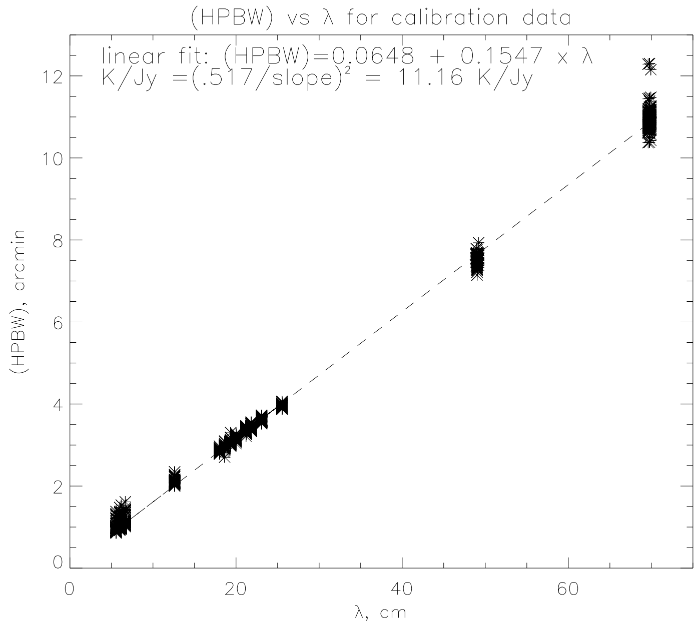

Fig. 5.— $(HPBW)$ vs λ for all calibration data in Sept 2000 except the C-band and 430CH systems.

We can determine $KperJy_{ideal}$ by fitting the wavelength dependence of the measured $HPBW$. Figure 5 shows the observations made during our calibration run, together with the results of the least squares fit. The data are very well fit by a straight line whose y-intercept is close to zero. Accordingly, $KperJy_{ideal} = 11.2$ K Jy^{-1}, the slope of the line. With a somewhat better telescope, we could *also* determine $KperJy_{ideal}$ by measuring it at low enough frequencies where the telescope is perfect.

If the blockage were 10%, then this measured value would also be 11.2 K Jy^{-1}. In fact, it is unlikely to be this high; theoretically calculated values are somewhat smaller. This would make the denominator in equation 18b smaller, and the numerator would also have to be smaller to retain the same measured $(HPBW)$; this corresponds to a slightly larger blockage. We believe that the blockage so derived would be the most accurate observationally-determined one.

4. MAIN BEAM ELLIPTICITY AND COMA

4.1. The Elliptical Main Beam

Arecibo's beam is elliptical by design; $\phi_{\rm beam}$ should be 90°, meaning that the za beam is larger than the az beam. Typically, $\Theta_1 \sim 0.1 \rightarrow 0.3$ and exhibits both az and za dependence. It is somewhat surprising that ϕ_{beam} exhibits systematic departures from 90°. ϕ_{beam} ranges from $\sim 80^\circ \rightarrow 110^\circ$ and does not get noticeably worse with frequency.

Figure 6 exhibits some typical data. For the two LBW graphs, both on B1749+096 (and taken simultaneously), the ellipticity is larger and the position angle deviates more from 90° than at 2380 MHz (source B2249+185). This, together with the absence of clear frequency dependence, suggests that the beam ellipticity is related to the telescope structure, for example asymmetric shadowing of the telescope beam by the triangle.

4.2. Coma

The coma lobe gets worse with frequency, with strength $\alpha_{\rm coma}$ rising from about 0.015 to 0.15 from 430 to 4500 MHz (at $za \sim 10^\circ$). At the higher frequencies it gets worse with za; at 4500 MHz $\alpha_{\rm coma}$ is, very roughly, linearly proportional to za, rising to ~ 0.25 at $za = 20^\circ$.

The direction ϕ_{coma} exhibits no clear systematic departure from being constant as a function of (az, za) or frequency. We illustrate this with Figure 7, which exhibits ϕ_{coma} for all calibration observations we took in September 2000 that had $\alpha_{coma} > 0.01$: ϕ_{coma} scatters about $\phi \sim 25^\circ$. ϕ_{coma} is defined in Figure 1; its zero point is fixed with respect to the azimuth arm. Its constancy shows that, in large measure, the coma is tied to the azimuth arm; this presumably indicates that it is the result of subreflector misalignment.

5. ϕ STRUCTURE IN THE FIRST SIDELOBE

We introduced the Fourier decomposition of the first sidelobe in section 2.3; we obtained a series with 8 points and we use 6 to reconstruct the sidelobe. This allows us to reconstruct Fourier components zero to three. Figure 8 exhibits the az dependence of these components.

The average amplitude (the zeroth Fourier component, top panel) seems to increase slightly near transit, which might reflect the slightly increased blockage that occurs there.

The position angles of the first and third Fourier components exhibit a striking dependence with az: the points follow the slope of the dotted line, meaning that these components are fixed with respect to the ground. The third Fourier component would respond to blockage by the triangle structure; its az dependence implies that it is doing just that. The interpretation for the

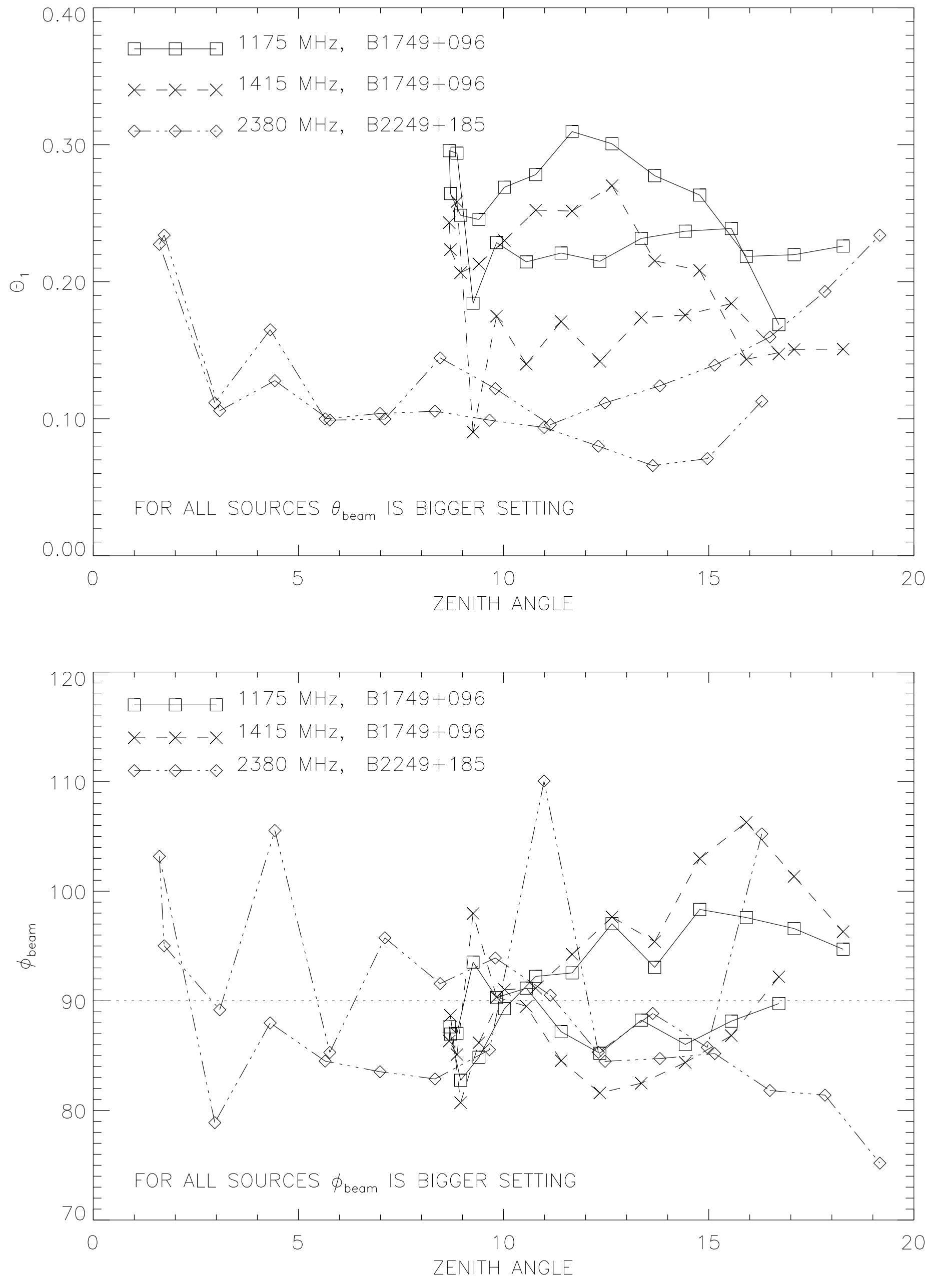

Fig. 6.— The main beam ellipticity Θ_1 and its position angle ϕ_{beam} (see equation 1) versus za, for three frequencies.

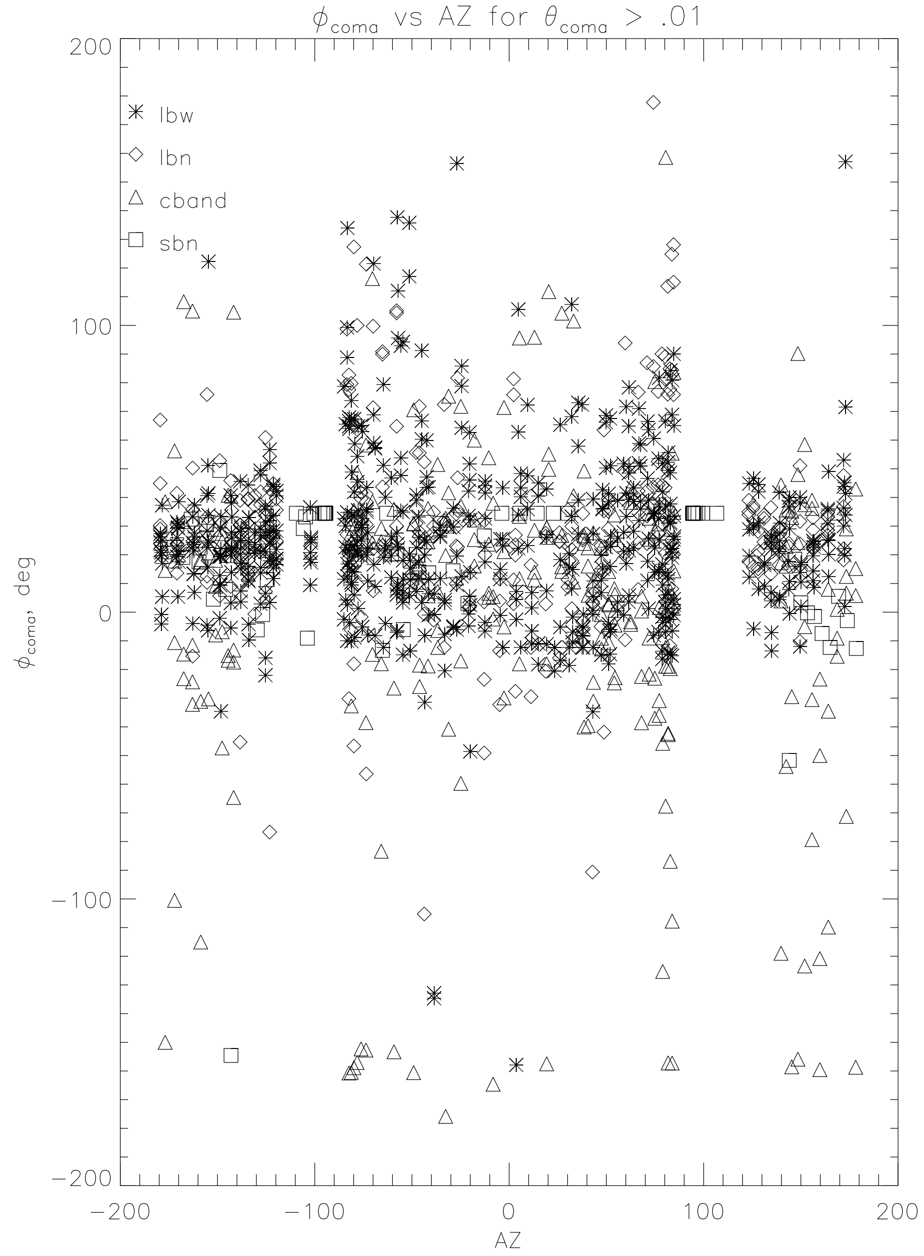

Fig. 7.— az dependence of ϕ_{coma} for the receivers above 1 GHz.

first Fourier component is less obvious.

The position angles of the second Fourier component are independent of az, implying that they are fixed with respect to the azimuth arm. This is consistent with the blockage of the azimuth

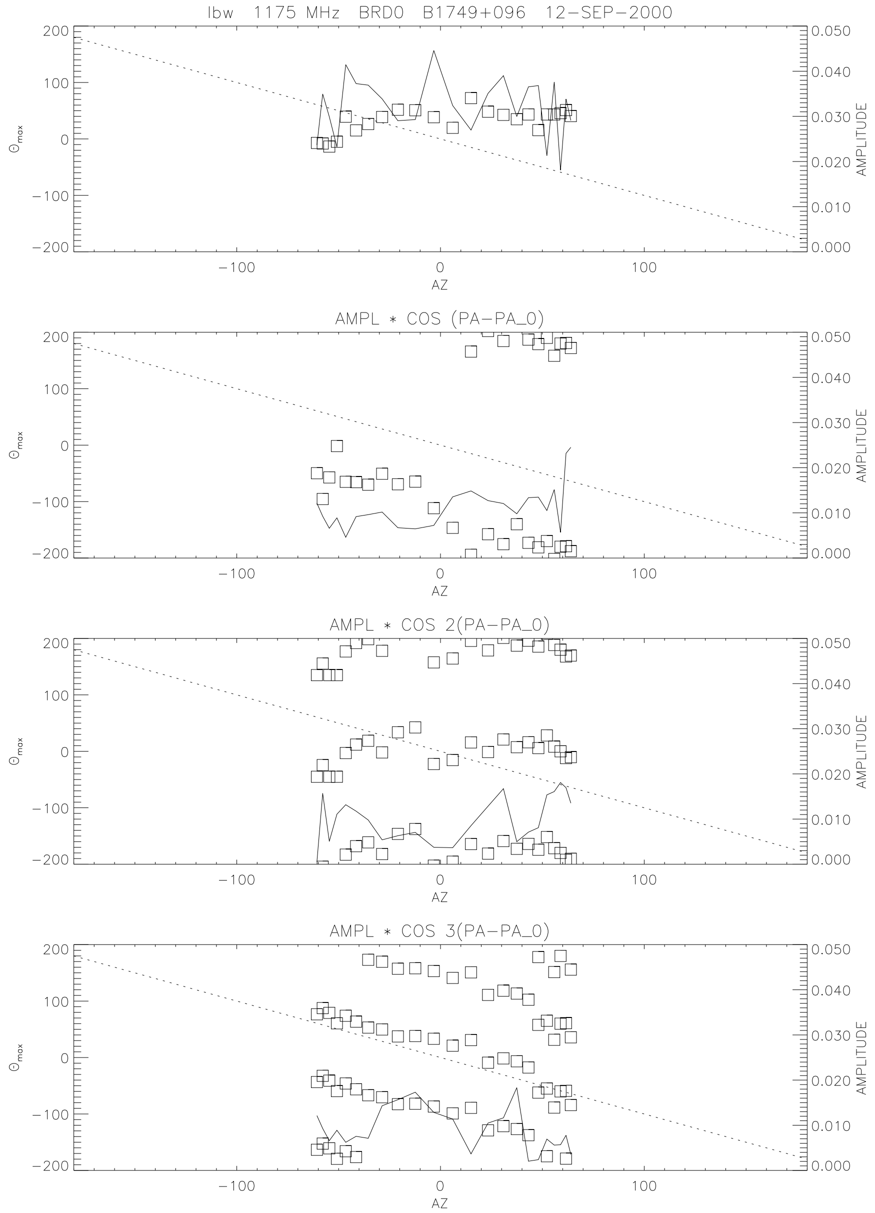

Fig. 8.— az dependence of the first three Fourier components of the first sidelobe in Stokes I for LBW at 1175 MHz. The dotted lines correspond to a component being fixed with respect to the ground. Solid lines are amplitude and the points are position angle ϕ_{max}, which is the angle ϕ at which the component peaks (ϕ is defined in Figure 1; here ϕ_{max} is labeled "POS ANGLE"). For the nth Fourier component, each point occurs n times over each 360° interval in ϕ, and all of those possibilities are plotted to better clarify the az dependence.

arm, which is a linear structure roughly centered on the illumination pattern and should produce a second Fourier component.

6. THE POLARIZED STOKES PARAMETERS

In ATOMS 99-02 we discussed beam squint and beam squash, terms that describe polarization of the main beam. Each Stokes parameter has its squint and squash. Beam squint is the difference in beam direction between orthogonal polarizations and is represented by $\frac{\partial P_n}{\partial \theta}$. Beam squash is the difference in beamwidth between orthogonal polarizations and is represented by $\frac{\partial P_n}{\partial \Theta}$.

To be more precise, consider Stokes Q as an example, which is polarization X minus Y. We define the normalized power pattern for a polarization X as $\frac{G_X}{G_{max}}$.[1] Then the power received from the source in each polarization is

$$P_X = S_X \exp\left(-\frac{(\theta + \frac{\delta\theta_Q}{2})^2\left(1 - \alpha_{\rm coma}\frac{\theta_{\rm coma}}{\Theta_0}\right)}{\left(\Theta + \frac{\delta\Theta_Q}{2}\right)^2}\right) \tag{19a}$$

$$P_Y = S_Y \exp\left(-\frac{(\theta - \frac{\delta\theta_Q}{2})^2\left(1 - \alpha_{\rm coma}\frac{\theta_{\rm coma}}{\Theta_0}\right)}{\left(\Theta - \frac{\delta\Theta_Q}{2}\right)^2}\right) . \tag{19b}$$

where S_X and S_Y are the source fluxes in the two polarizations. Recall that Θ, θ_Q, and Θ_Q all depend on ϕ. The unsubscripted P is the sum (Stokes I), while the difference gives the measured Stokes Q:

$$P_Q = QP_n + \frac{I}{2}\left[\frac{\partial P_n}{\partial \theta_Q}\delta\theta_Q(\phi) + \frac{\partial P_n}{\partial \Theta_Q}\delta\Theta_Q(\phi)\right] . \tag{20}$$

The quantities $\delta\theta_Q(\phi)$ and $\delta\Theta_Q(\phi)$ are not themselves the beam squint and squash. Rather, the squint and squash are represented by (magnitude, position angle), $(\theta_{squint}, \phi_{squint})$ and $(\theta_{squash}, \phi_{squash})$, and are given by

$$\delta\theta_Q = \theta_{squint}\cos(\phi - \phi_{squint}) \tag{21a}$$

$$\delta\Theta_Q = \Theta_{squash}\cos 2(\phi - \phi_{squash}) . \tag{21b}$$

[1] Recall that above we defined the unsubscripted G (which includes G_{max}) to apply to $\frac{\text{Stokes I}}{2}$.

The quantity $\delta\theta_Q$ varies as $\cos\phi$ because it is like a pointing offset and has a *direction*. In contrast, the quantity $\delta\Theta_Q$ varies as $\cos 2\phi$: in beam squash, the beamwidth varies as $\cos 2\phi$ so it only has an *orientation*.

6.1. Results for Beam Squint and Squash

We least-squares fit equation 20 to the data, regarding P_n as known. This is acceptable, even though P_n is itself a result of a least-squares fit, because its data are Stokes I with high S/N. We do this in all three Stokes parameters. Figures 9 and 10 show representative plots for Stokes (Q, U). The squint and squash amplitudes are in the few arcsecond range and there is significant variation, but no easily physically interpretable dependence, on (za, az). On the other hand, Stokes V (Figure 11) is more smoothly behaved: the squint is somewhat smaller and maintains a constant ϕ, while the squash is very small.

For the linearly polarized Stokes parameters (Q, U), we expect beam squash but no squint (Tinbergen 1996). The prediction regarding squints is not satisfied at all. Beam squints for Stokes (Q, U) are comparable to that for V. The behaviors of ϕ_{squint} for (Q, U) are uninterpretable in simple terms and provide no hint about the cause of the squint. The beam squash amplitude variations are also uninterpretable. The angles ϕ_{squash} should be fixed with respect to the azimuth arm; very roughly speaking, they are. However, they should differ by 45° between Q and U; they don't.

For Stokes V, one expects beam squint but no beam squash (see discussion by Troland and Heiles 1982). This prediction is reasonably well satisfied. The squint amplitude is roughly constant and its angle ϕ_{squint} is constant, fixed with respect to the azimuth arm as it should be. The squash is small, far smaller than for Stokes (Q, U), although it is not zero.

The reasons for the severe departure of Stokes (Q, U) from theory are completely unclear to us. The absence of a clearly defined dependence with on az suggests a combination of effects that are fixed with respect to the ground and the az arm; the obvious candidates are aperture blockage and secondary/tertiary mirror misalignment.

6.2. The effects of Beam Squint and Squash on Extended Sources

Suppose one is observing a large-scale feature where the brightness temperature T_B varies with position. One can express this variation by a two-dimensional Taylor expansion. The first derivative is described by a single term with a magnitude and direction; the second derivative is described three terms, $\frac{d^2T_B}{daz^2}$, $\frac{d^2T_B}{dza^2}$, $\frac{d^2T_B}{dazdza}$. **In this section and its figures, T_B refers to Stokes I so is twice is conventionally used value**.

Beam squint, by its nature, responds to the first derivative and only slightly to the second;

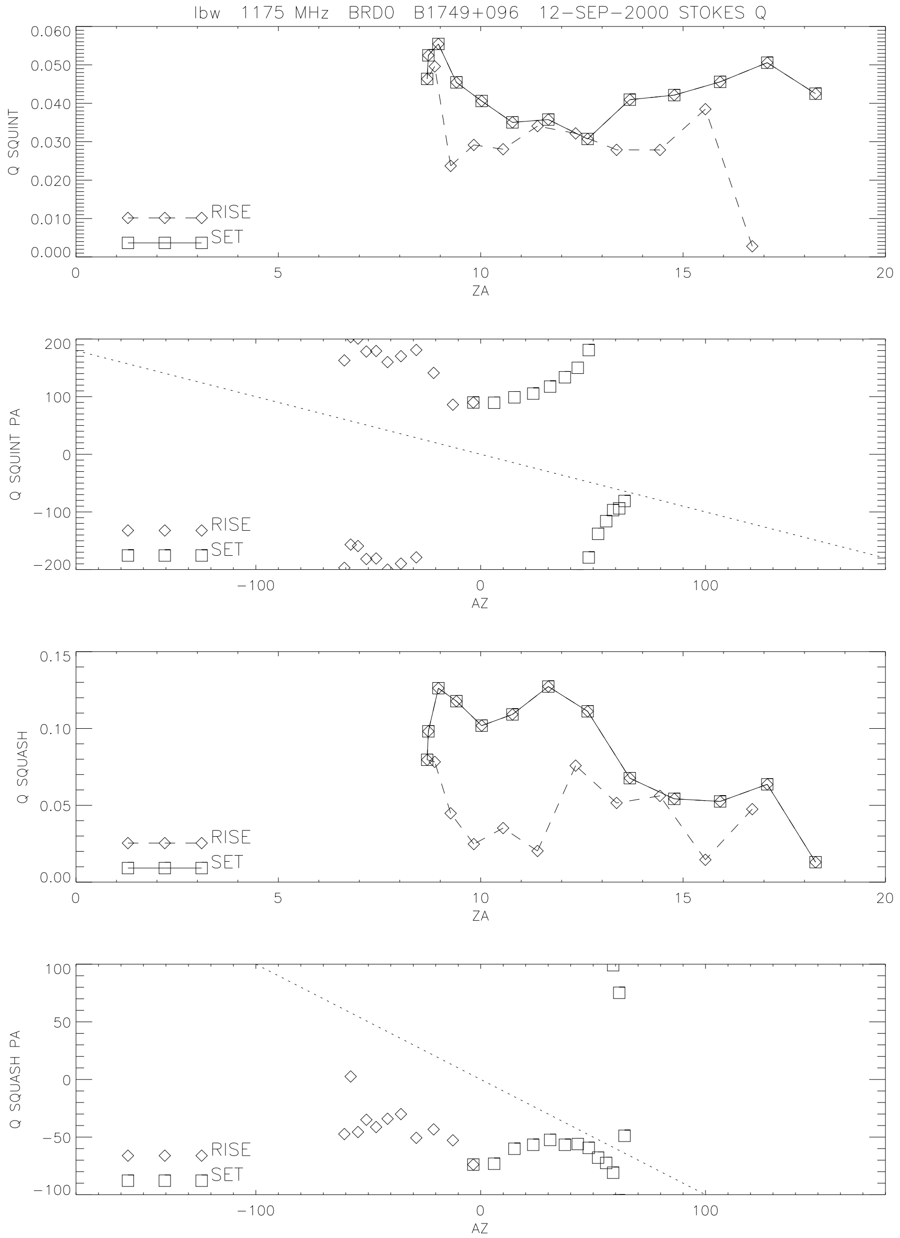

Fig. 9.— (za, az) dependence of amplitudes (in arcmin) and $(\phi_{squint}, \phi_{squash})$ of beam squint and squash for Stokes Q. (Here ϕ is labeled "PA"). The dotted line corresponds to being fixed with respect to the sky or ground. **In this figure, Q is oriented 45° to the azimuth arm and fixed with respect to it.**

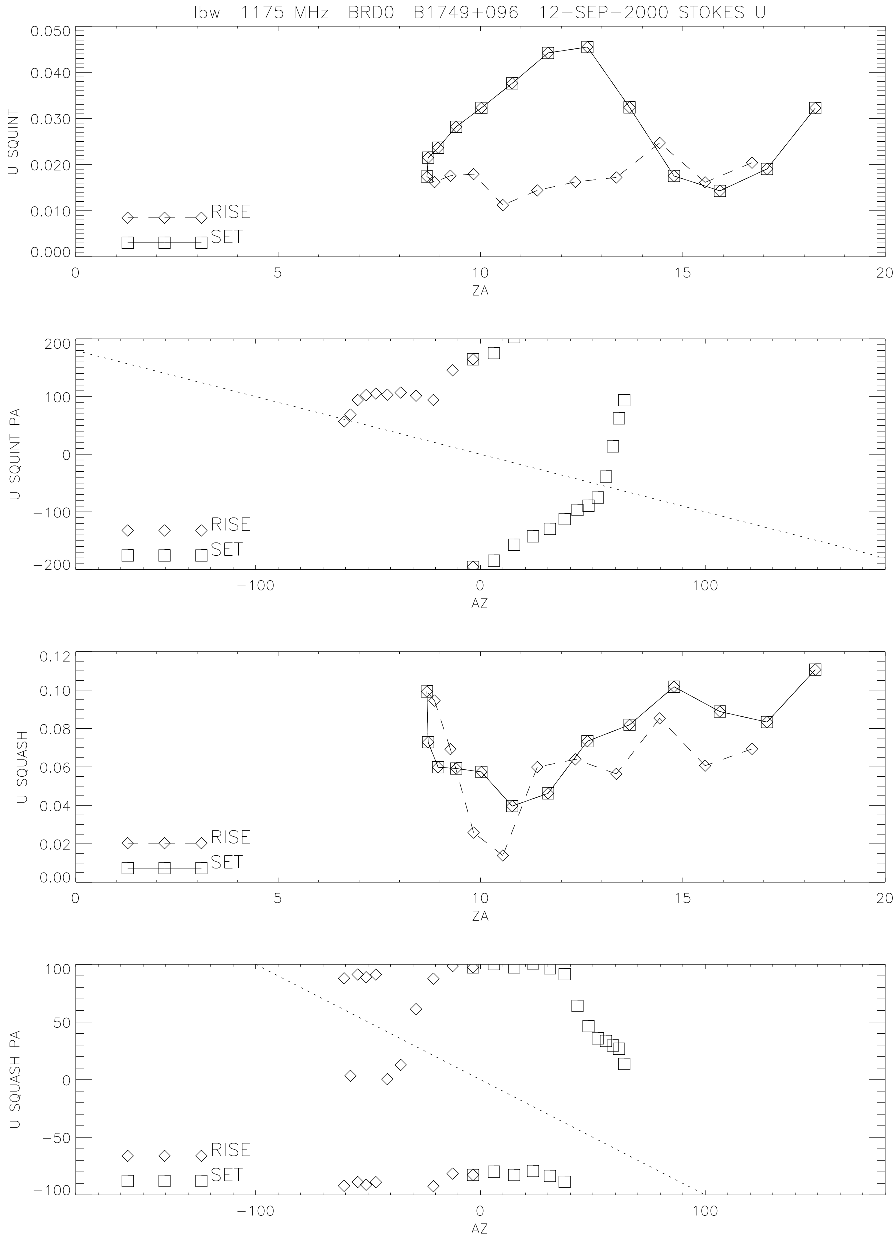

Fig. 10.— (za, az) dependence of amplitudes (in arcmin) and $(\phi_{squint}, \phi_{squash})$ of beam squint and squash for Stokes U. (Here ϕ is labeled "PA"). The dotted line corresponds to being fixed with respect to the sky or ground. **In this figure, U is aligned with the azimuth arm and fixed with respect to it.**

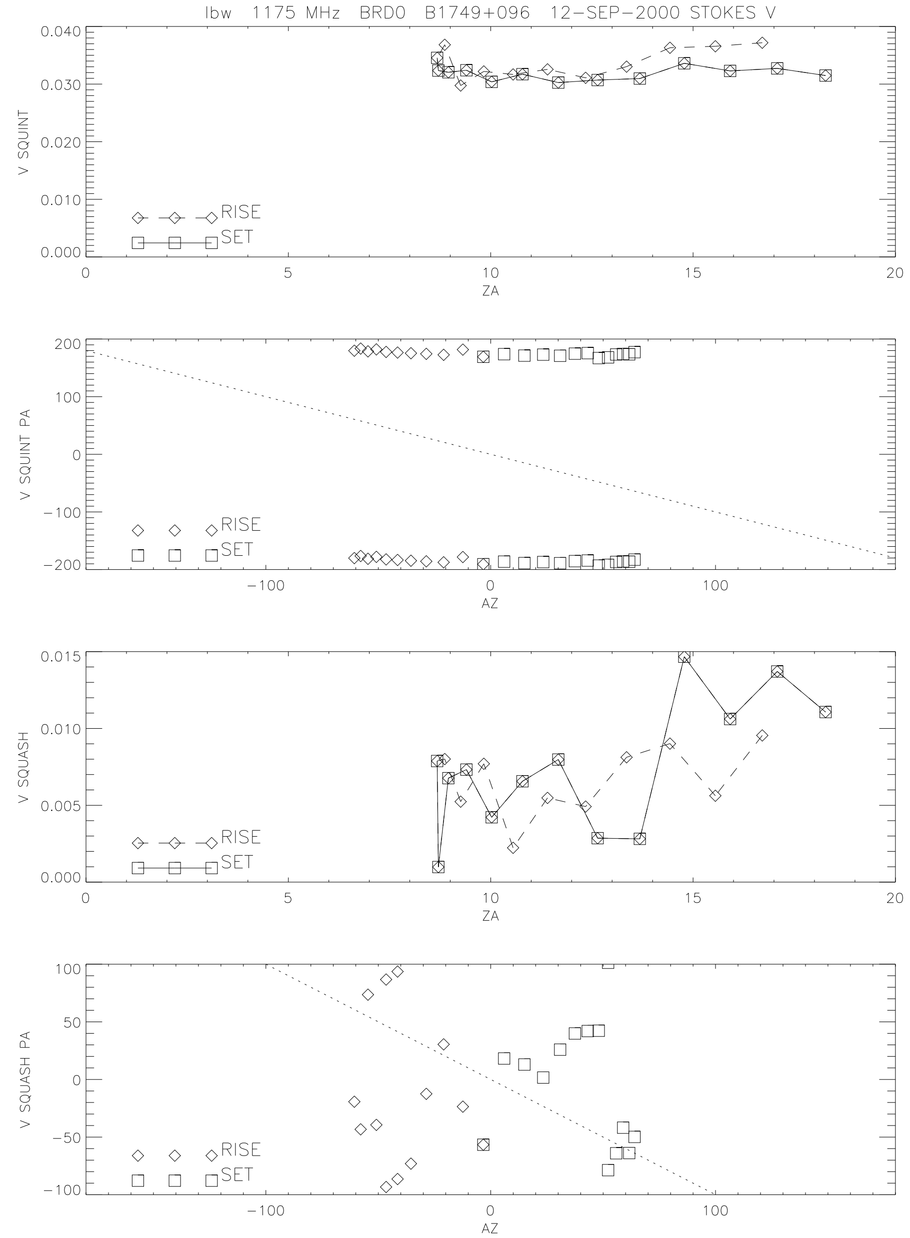

Fig. 11.— (za, az) dependence of amplitudes (in arcmin) and $(\phi_{squint}, \phi_{squash})$ of beam squint and squash for Stokes V. (Here ϕ is labeled "PA"). The dotted line corresponds to being fixed with respect to the sky or ground.

beam squash responds primarily to the second. To illustrate the effects of polarized beam structure, we present plots of the response of the polarized beam to these derivatives. In these plots we adopt derivatives of 1 K arcmin^{-1} and 1 K arcmin^{-2} to facililtate scaling to other measured derivatives, not because these values are necessarily realistic; also, In these figures the brightness temperatures refer to Stokes I, not $\frac{I}{2}$, so they are twice the conventionally used values. The response comes from three separable causes: main beam squint, main beam squash, and the first sidelobe polarization structure. We show these responses individually and, also, we show the total response.

Figures 12 and 13 show Stokes Q and U. In these two figures, the position angles PA are defined *on the sky with the conventional astronomical definition.* For the first-derivative case, the dominant contribution comes from the first sidelobe, which contributes far more than the main beam squint. The amplitudes are roughly constant with az. The angles of maximum response are, *very* roughly, fixed on the sky (they change less rapidly than az), which is consistent with the first sidelobe's effects being caused by blockage. For the second derivative case, the first sidelobe contribution dominates over main beam squash, but not by much.

Figure 14 shows the Stokes V result. In this figure, PA is the angle of maximum response *defined relative to the azimuth arm.* The total amplitudes for both derivatives are smaller by a factor $\sim$ 10 than for Stokes (Q,U). For the first derivative, the PA is independent of az, as expected from the squint result. The sidelobe is again the dominant contribution, but not overwhelmingly so: in fact, its amplitude is about twice that of the main beam squint but the direction is opposite. This has the curious effect of making the *amplitude* of the total beam response about the same with and without the sidelobe—but reversing the *direction* of gradient for maximum response! For the second derivative, the first sidelobe and main beam squash contribute comparably and the PA behavior is correspondingly complicated.

We emphasize that these particular results can produce serious systematic errors when measuring the polarization of extended emission. The results represented in Figures 12, 13, 14 are contributions in the *polarized* Stokes parameters (Q,U,V) that arise from spatial gradients in the *total intensity* Stokes parameter I. The fractional polarization of extended emission tends to be small, so spatial gradients in I can be very serious. Correcting for them is a complicated business because of the PA variation with (az,za). It is also an uncertain business, especially for (Q,U) and somewhat less so for V, because these variations are unpredictable and must be determined empirically.

In that spirit, these plots are more useful as guides of what can be reliably measured than they are for correction of the measurements. Consider, for example, measuring Zeeman splitting of the 21-cm line in emission, which involves measuring Stokes V. Figure 14 shows that a brightness temperature gradient $\frac{dT_B}{d\theta}$ = 1 K arcmin^{-1} produces an artificial temperature $T_{\rm art} \sim 0.04$ K response in Stokes V; let this ratio be denoted by $\mathcal{K} \equiv \frac{V_{\rm art}}{dT_B/d\theta} \sim 0.04$. Then it's easy to show that, for a Landé g factor 2.8 Hz μG^{-1}, $B_{\rm art} = 1690\mathcal{K}\frac{dv}{d\theta}$ μG, where $\frac{dv}{d\theta}$ is the velocity gradient in km s^{-1} arcmin^{-1}. For a representative $\frac{dv}{d\theta}$ = 1 km s^{-1} deg^{-1} we get $B_{\rm art} \sim 2.3$ μG. Heiles (1996) presents statistics of the velocity gradient measured with a 36 arcmin $HPBW$; gradients of 1 km

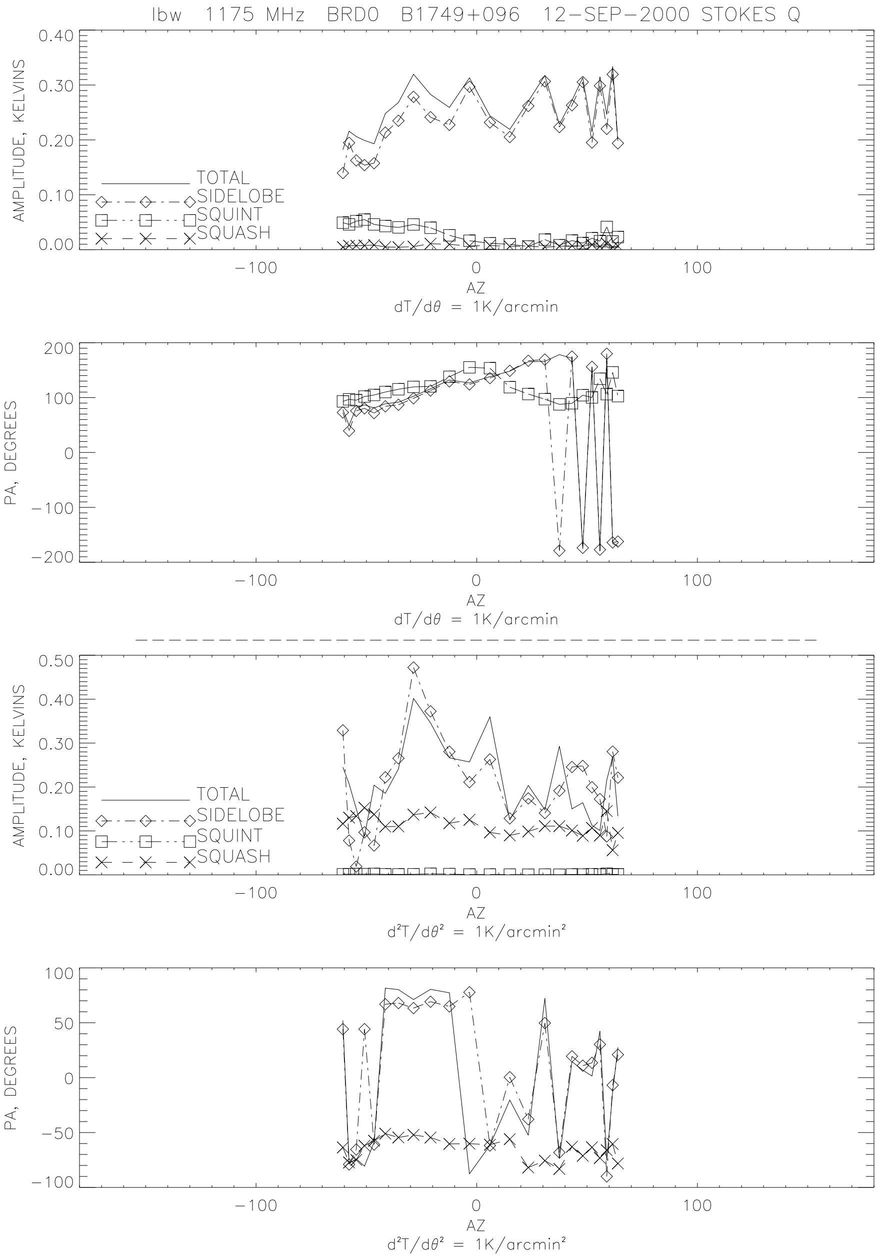

Fig. 12.— az dependence of the telescope's response to the first spatial derivative in brightness temperature (top two panels) and to the second derivative (bottom two panels), all for Stokes Q. PA is direction of maximum response. **In this figure, Q and PA are defined on the sky with the conventional astronoomical definition.** T_B refers to Stokes I so is twice is conventionally used value.

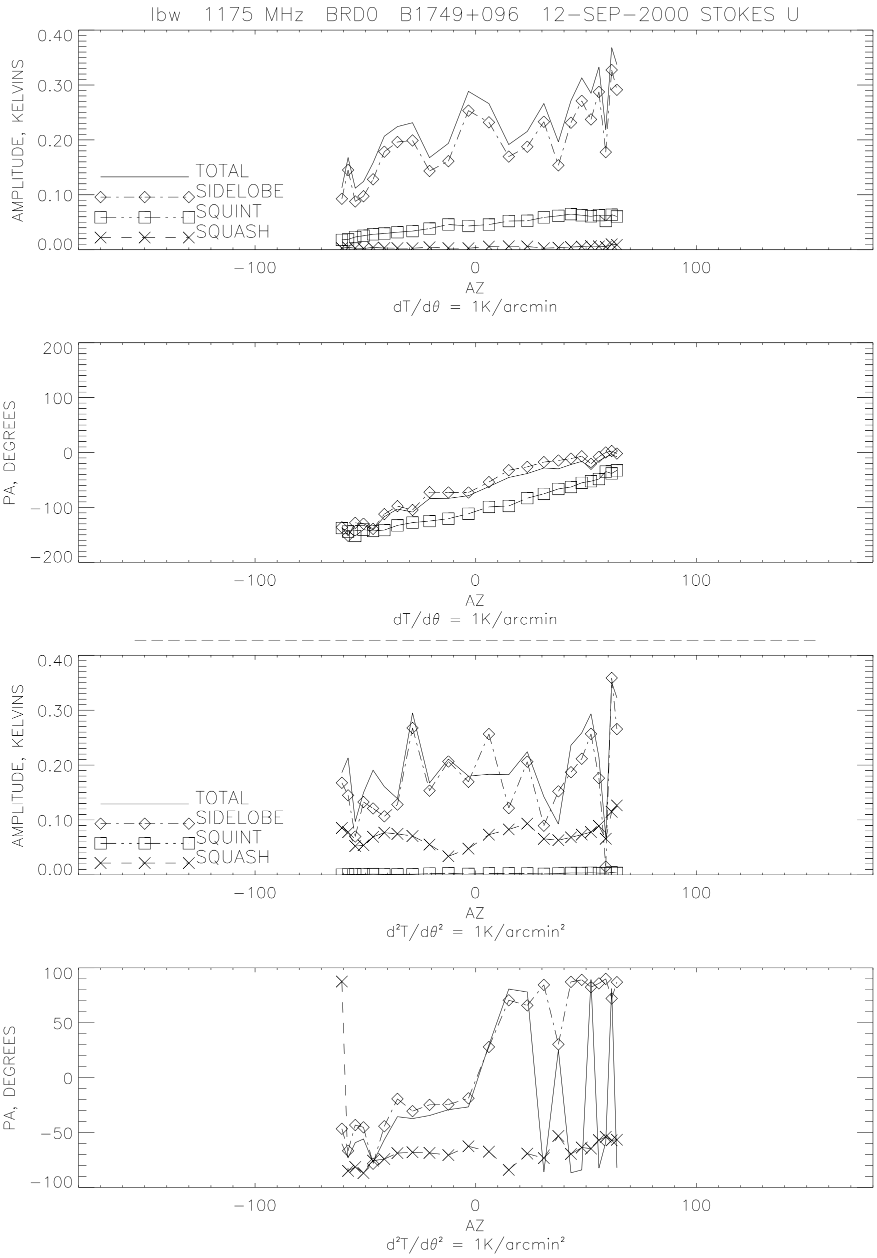

Fig. 13.— *az* dependence of the telescope's response to the first spatial derivative in brightness temperature (top two panels) and to the second derivative (bottom two panels), all for Stokes U. PA is direction of maximum response. **In this figure, U and PA are defined on the sky with the conventional astronoomical definition.** T_B refers to Stokes I so is twice is conventionally used value.

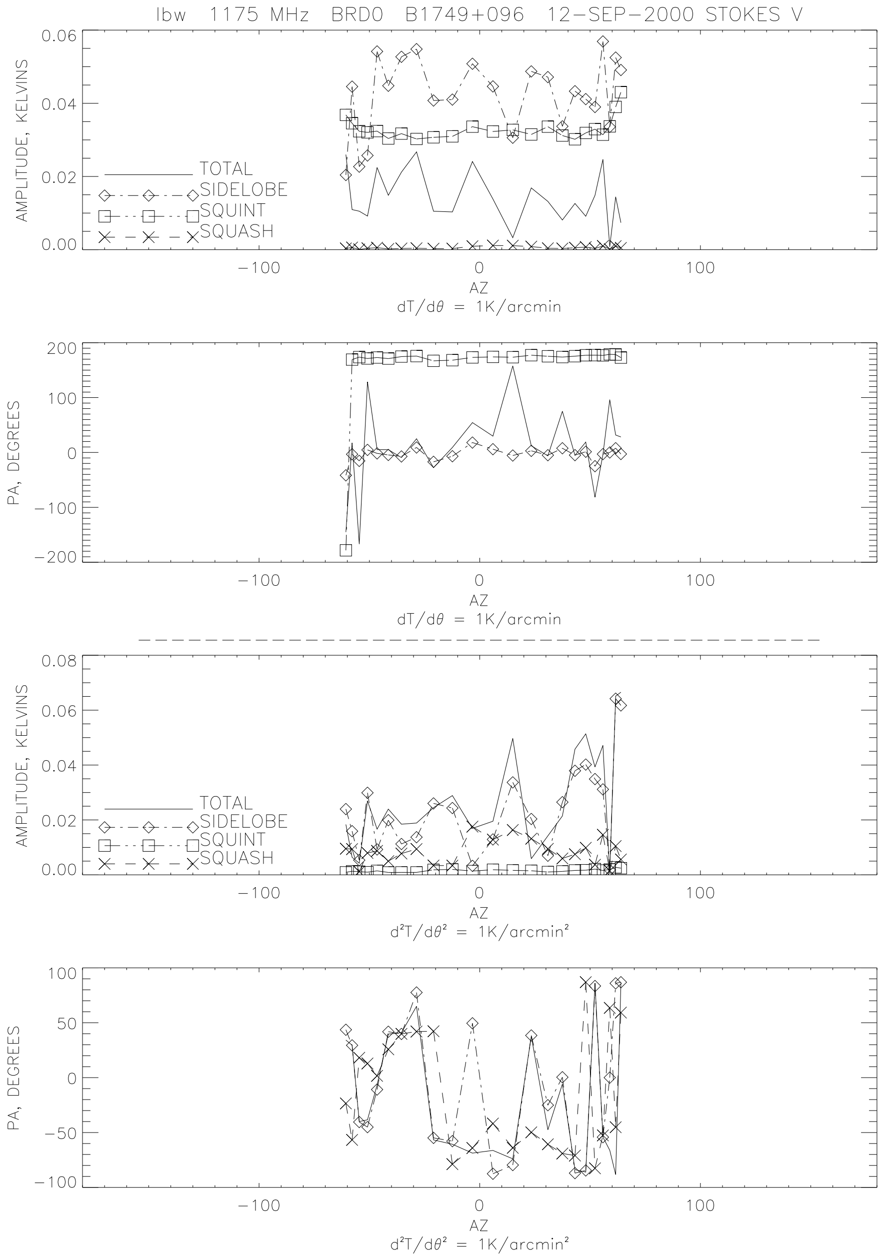

Fig. 14.— *az* dependence of the telescope's response to the first spatial derivative in brightness temperature (top two panels) and to the second derivative (bottom two panels), all for Stokes V. PA is the ϕ of maximum response, **defined relative to the azimuth arm as in Figure 1**. T_B refers to Stokes I so is twice is conventionally used value.

s^{-1} deg^{-1} are not uncommon. Typical values of B are in the μG range, so this effect can be—but is not always—serious!

7. IMAGES OF THE BEAM IN ALL STOKES PARAMETERS

It's all well and good to parameterize the beams; it's especially appropriate for quantitative work. However, for getting a feel for the situation there's nothing like an image. So here we provide images for one of our many hundreds of beam maps. As for our previous figures, these images are all for LBW (1175 MHz) observing B1749+096; it was setting, with $(az, za) \approx (64^\circ, 18.4^\circ)$.

The main beam parameters are as follows:

For Stokes I, $(\Theta_0, \Theta_1) = (4.00, 0.36)$ arcmin (both are HPBW); $\phi_{\rm beam} = 91.1^\circ$; $\alpha_{\rm coma} = 0.048$; $\phi_{\rm coma} = 41.4^\circ$; mean height of first sidelobe= 0.029.

For Stokes Q, $(\theta_{squint}, \phi_{squint}) = (0.019', -173^\circ)$ and $(\Theta_{squash}, \phi_{squash}) = (0.11', 19^\circ)$. As in Figure 9, Q is oriented 45° to the azimuth arm.

For Stokes U, $(\theta_{squint}, \phi_{squint}) = (0.056', -42^\circ)$ and $(\Theta_{squash}, \phi_{squash}) = (0.061', -47^\circ)$. As in Figure 10, U is aligned with the azimuth arm.

For Stokes V, $(\theta_{squint}, \phi_{squint}) = (0.045', -10^\circ)$ and $(\Theta_{squash}, \phi_{squash}) = (0.007', 37^\circ)$.

The beam is considerably elliptical, which is a result of the high zenith angle. The Stokes Q beam shows the classic four-lobed pattern, beam squash, for linear polarization; in contrast, the U beam is polluted with a large unpredicted squint and a huge linearly polarized sidelobe. Theoretically, the beam squashes in (Q, U) must be aligned with their orientations, and in particular the two four-lobed patterns should be rotated 45° with respect to each other; this is not the case! The V beam is reasonably well-behaved. We commented on these aspects in more detail above.

This work was supported in part by NSF grant 95-30590 to CH.

REFERENCES

Heiles, C. 1996, ApJ, 466, 224.

Rohlfs, K. & Wilson, T.L. 2000, Tools of Radio Astronomy, Springer-Verlag, chapters 5, 6.

Ruze, J. 1966, Proc. IEEE 54, 633.

Tinbergen, J. 1996, Astronomical Polarimetry, CU Press, p. 82.

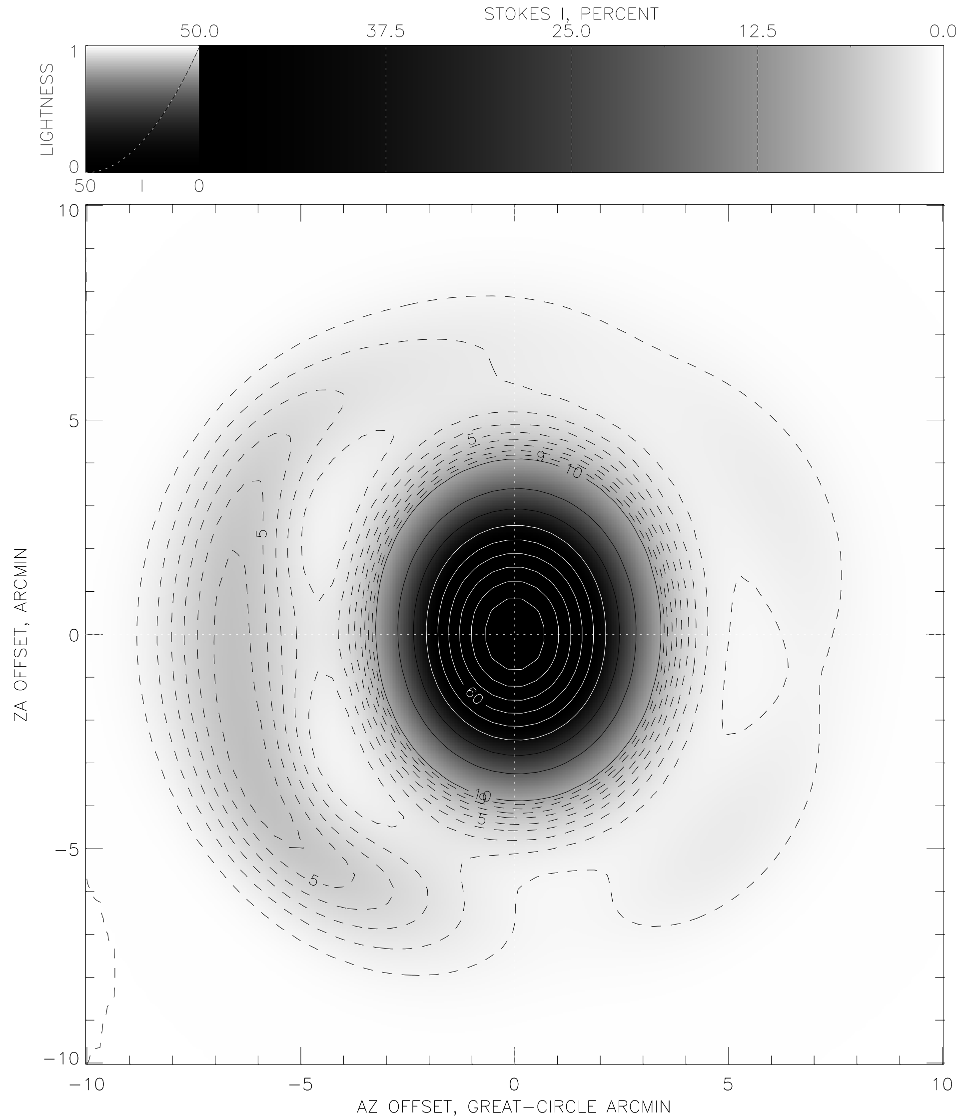

Fig. 15.— Grey-scale/contour of the Stokes I main beam and first sidelobe reconstructed from the derived parameters. Solid contours are $(0.1, 0.2, \ldots)$ of the peak; dashed contours are $(0.01, 0.02, \ldots)$.

Troland, T.H. & Heiles, C. ApJ, 252, 179.

This preprint was prepared with the AAS LaTeX macros v4.0.

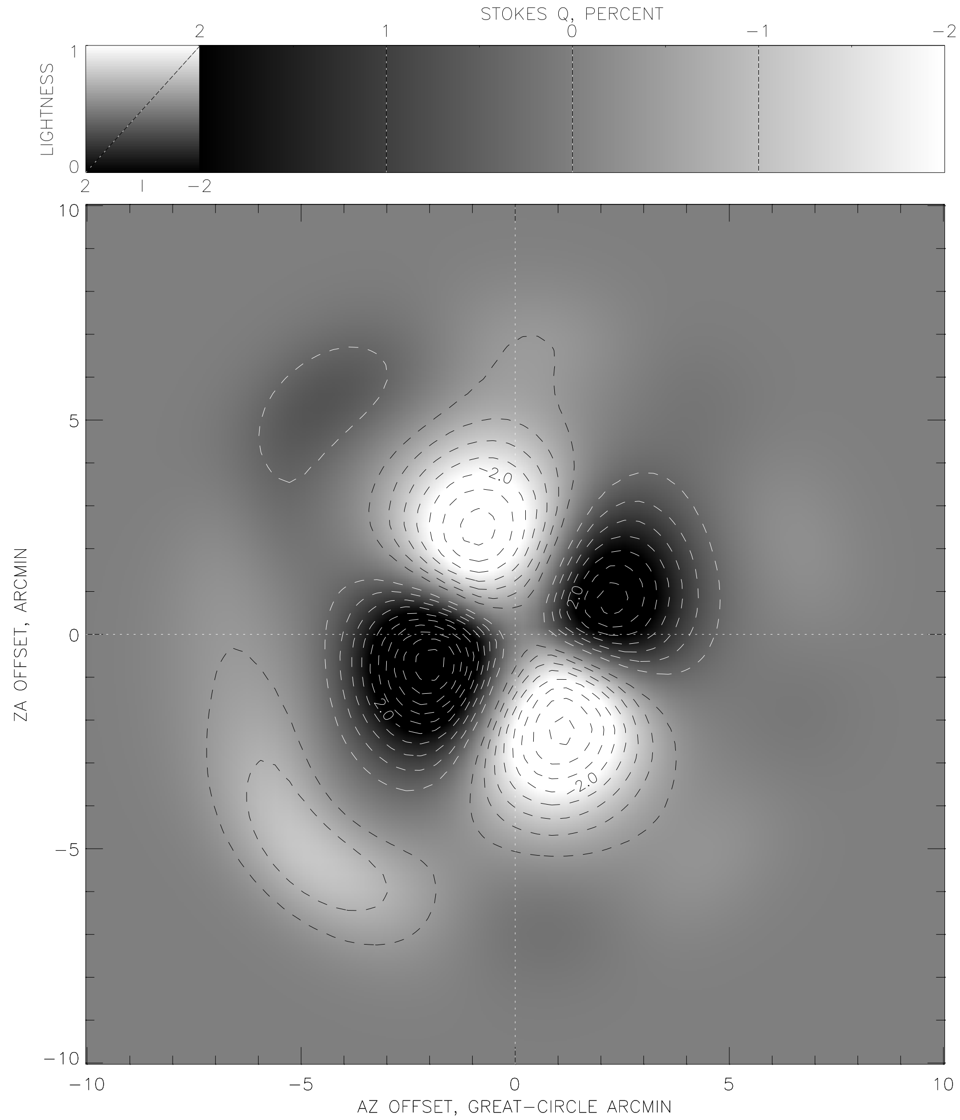

Fig. 16.— Grey-scale/contour of the Stokes Q main beam and first sidelobe reconstructed from the derived parameters. Black contours are for areas with negative Q with the grey scale tending towards white; white contours are positive Q with the greyscale tending towards black. Contours are in percent of Stokes I and spaced by 0.4%; the 0% contour is omitted. As in Figure 9, Q is oriented 45° to the azimuth arm.

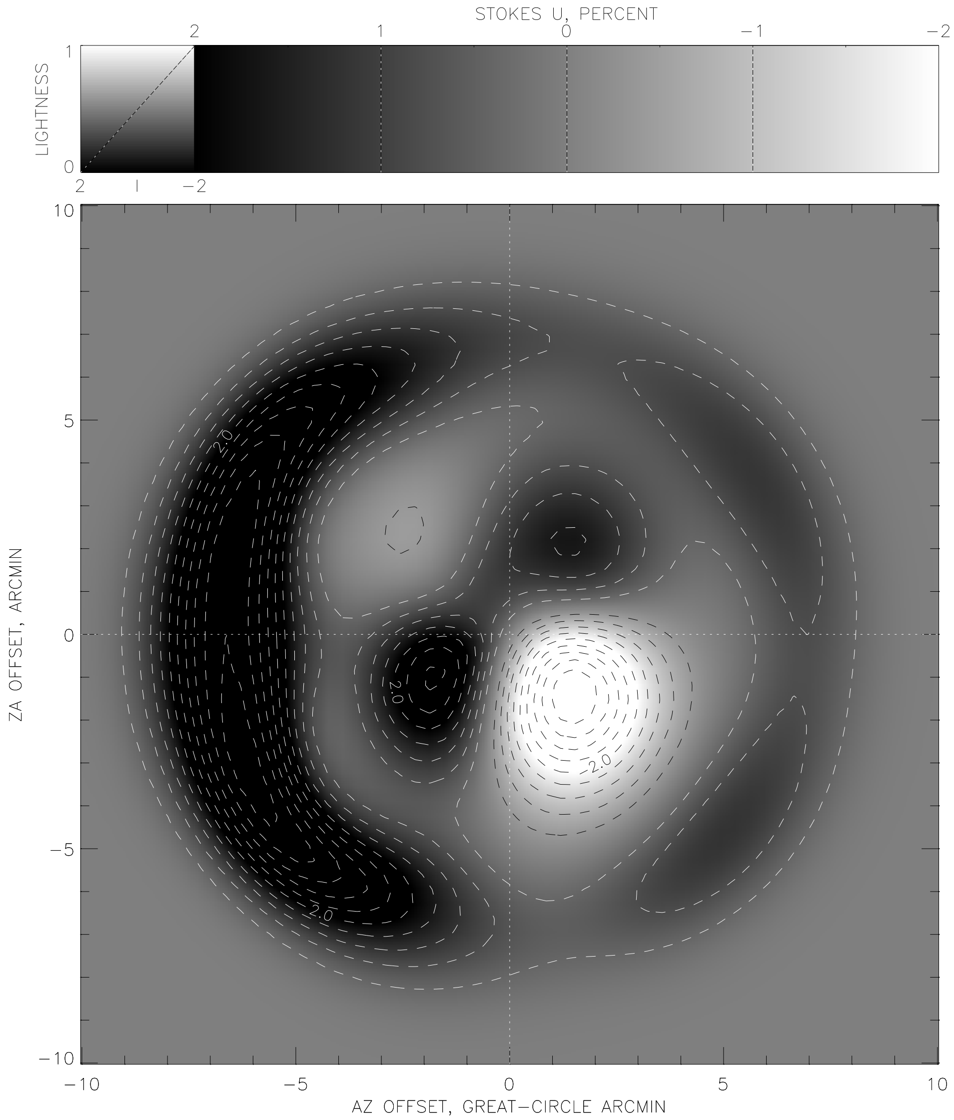

Fig. 17.— Grey-scale/contour of the Stokes U main beam and first sidelobe reconstructed from the derived parameters. Black contours are for areas with negative U with the grey scale tending towards white; white contours are positive U with the greyscale tending towards black. Contours are in percent of Stokes I and spaced by 0.4%; the 0% contour is omitted. As in Figure 10, U is aligned with the azimuth arm.

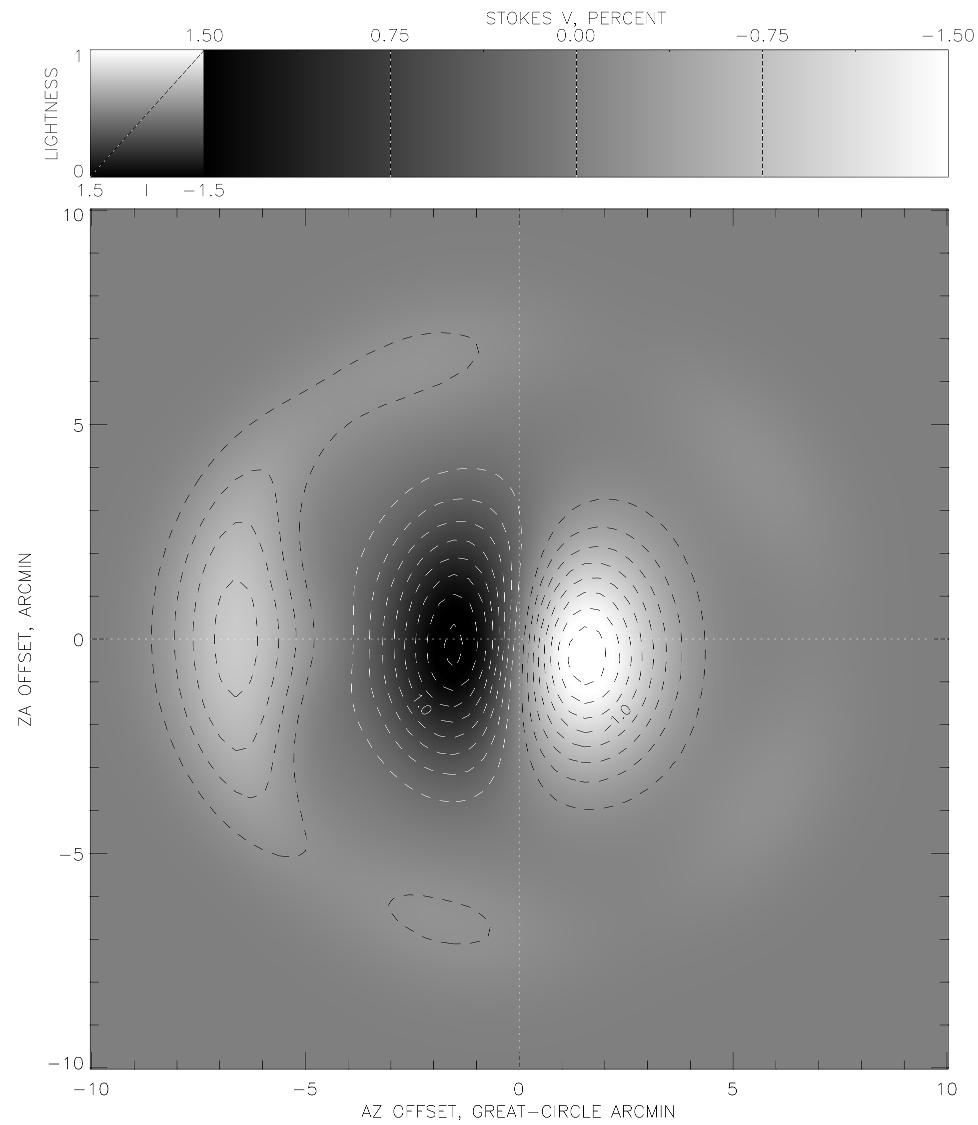

Fig. 18.— Grey-scale/contour of the Stokes V main beam and first sidelobe reconstructed from the derived parameters. Black contours are for areas with negative V with the grey scale tending towards white; white contours are positive V with the greyscale tending towards black. Contours are in percent of Stokes I and spaced by 0.2%; the 0% contour is omitted.